Journal of Solid State Chemistry 227 (2015) 92–97

Contents lists available at ScienceDirect

Journal of Solid State Chemistry

journal homepage: www.elsevier.com/locate/jssc

Stabilization of the $Ti_3Co_5B_2$-type structure for $Ti_{3-x}Si_xRu_5B_2$ through Si–Ti substitution

Weiwei Xie*, M.K. Fuccillo, B.F. Phelan, H. Luo, R.J. Cava

Department of Chemistry, Princeton University, Princeton, NJ 08540, United States

ARTICLE INFO

Article history:
Received 17 November 2014
Received in revised form
27 March 2015
Accepted 29 March 2015
Available online 4 April 2015

Keywords:
Boride
Structural stability
Physical properties

ABSTRACT

We report a route for designing and synthesizing $Ti_3Co_5B_2$-type compounds in the Ti–Ru–B system by using chemical substitution of Si for Ti to decrease the *d*-electron-based antibonding interactions that it is argued would otherwise drive an instability in this structure for unsubstituted $Ti_3Ru_5B_2$. $Ti_{3-x}Si_xRu_5B_2$ with $x=0.75$, 1.00 and 1.25 nominal compositions crystalizes in the $Ti_3Co_5B_2$ structure type using arc melting methods, whereas at lower doping levels ($x=0.0$, 0.25 and 0.50) the more complex $Zn_{11}Rh_{18}B_8$-type structure is stable. Electronic structure calculations show that in hypothetical, unsubstituted $Ti_3Ru_5B_2$ with the $Ti_3Co_5B_2$-type structure, the antibonding interactions are strong around the Fermi level between the Ti and Ru in the structure that form tetragonal prisms. We propose that weakening these strong interactions through the partial substitution of isovalent Si for Ti leads to the observed stability of the $Ti_3Co_5B_2$-type structure for $Ti_{3-x}Si_xRu_5B_2$ for $x \approx 1$.

Published by Elsevier Inc.

1. Introduction

In the past two decades a series of metal-rich borides has been synthesized that contains magnetically active 3*d* atoms in close proximity to each other, resulting in studies of their magnetic exchange interactions [1–6]. Some of these compounds are variants of the related $Ti_3Co_5B_2$-type and $Zn_{11}Rh_{18}B_8$-type structures, both of which are tetragonal, crystallizing in the space group *P*4/*mbm* [7,8]. The $Ti_3Co_5B_2$-type structure, shown in Fig. 1a, contains trigonal, tetragonal, and pentagonal prisms of Co surrounding Ti and B. The $Zn_{11}Rh_{18}B_8$-type, on the other hand (Fig. 1b), which for comparison purposes may be written as $Zn_{2.75}Rh_{4.5}B_2$, is more complex, with a 2×2 superlattice of the $Ti_3Co_5B_2$-type in the tetragonal *ab* plane that is due to both minor atom deficiencies and the displacements of Zn–Rh neighbors. Previous work shows the valence electrons indeed play a crucial role in the stability of $Ti_3Co_5B_2$-type phases [2]. For example, substitution of Co by valence-electron-deficient Ru, along with the substitution of Ti by valence-electron-rich Nb, leads to the previously reported compound, $Nb_3Ru_5B_2$ [9]. Recent research has shown that $Nb_3Ru_5B_2$ is stable mainly because the Nb–Ru interactions between neighboring tetragonal prisms are strongly bonding and thus overtake the Nb–Ru antibonding interactions in the pentagonal prisms [9]. In contrast to what is found in the Nb–Ru–B system, in the Ti–Ru–B system the compound that forms, $(Ti_{10.05}Ru_{0.95})Ru_{18}B_8$, has the $Zn_{11}Rh_{18}B_8$-type structure rather than the $Ti_3Co_5B_2$-type structure [10]. Although it is usually assumed that such differences are the result of a difference in valence electron count, here we ask "What drives the ternary Ti–Ru–B compound to distort from the $Ti_3Co_5B_2$-type to the $Zn_{11}Rh_{18}B_8$-type? Is it only valence electron counting? Or is it something else?" [11,12].

Early research has shown that Si doping can be used to change the electron count in other $Ti_3Co_5B_2$-type compounds [13]. Here we have made an electron-count conserving substitution, using Si to partially replace Ti in the system to form $Ti_{3-x}Si_xRu_5B_2$, which has the same valence electron count as the hypothetical $Ti_3Ru_5B_2$. Ti and Si are quite different chemically, especially due to the lack of *d* valence electrons in Si. Dramatically, the substitution results in $Ti_{3-x}Si_xRu_5B_2$ (for *x* near 1) crystallizing in the $Ti_3Co_5B_2$-type structure. The analysis of the electronic structures of two model compounds, $Ti_2SiRu_5B_2$ and "$Ti_3Ru_5B_2$" in the $Ti_3Co_5B_2$-type structure, indicates that strong Ti–Ru atomic interactions, which depend on the presence of the Ti 3*d* electrons, are the major factor that determines the stability of the structure, not the valence electron count. Thus strong atomic interactions are shown to result in a major instability separating two related structure types in this metal rich boride system.

2. Experiments and calculations

2.1. Synthesis

Polycrystalline samples were synthesized by arc melting the elements in a water-cooled copper crucible under an argon atmosphere using a tungsten electrode. The starting materials, titanium (powder, 99.9%, Alfa Aesar), vanadium (powder, 99.9%, Alfa Aesar),

* Corresponding author. Tel.: +1 515 509 0057.
E-mail address: weiweix@princeton.edu (W. Xie).

http://dx.doi.org/10.1016/j.jssc.2015.03.029
0022-4596/Published by Elsevier Inc.

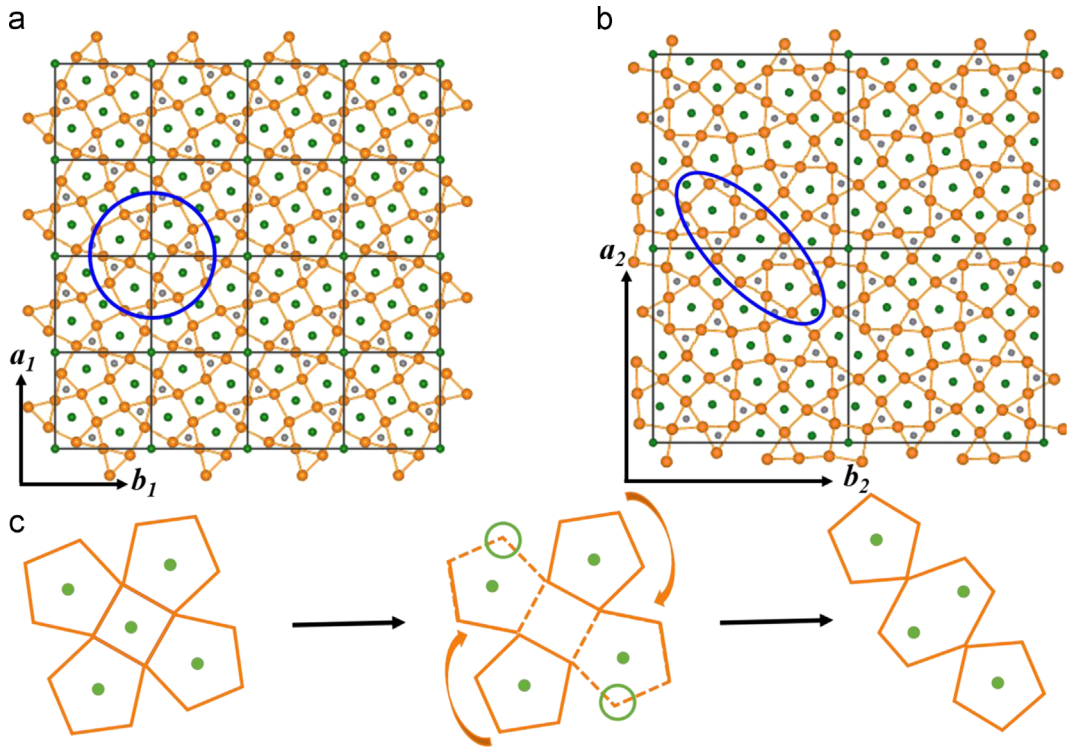

Fig. 1. Comparison of the $Ti_3Co_5B_2$ and $Zn_{11}Rh_{18}B_8$ structure types. The Co (Rh) atoms are shown in orange, the Ti (Zn) atoms are shown in green, and the B atoms are shown in grey. (a) The $Ti_3Co_5B_2$ structure. The true cell is outlined in black, but for comparison purposes, 4×4 unit cells in the *ab*-plane are shown. (b) The $Zn_{11}Rh_{18}B_8$ structure. The unit cell, which is $2 \times a$ and $2 \times b$ of the $Ti_3Co_5B_2$-type cell, is outlined in black. Four cells are shown to highlight the essential structural features. Blue ovals highlight the places where the structures differ most significantly. (c) The hypothetical structural evolution between phases. $Ti_{12}Ru_{20}B_8$ ($4 \times Ti_3Ru_5B_2$) (initial diagram) loses a Ti atom (central diagram) to break the strong atomic interactions in the tetragonal prism. After breaking the tetragonal prism, the Ru atoms on two of the vertices of the prism (circled in green) are expelled. The atoms then rearrange to form a doubly occupied, distorted hexagonal prism (final diagram). The $4 \times$ Ti3Ru5B2 → Ti11Ru18B8 + TiRu2 evolution is analogous to an elimination reaction in organic chemistry. (For interpretation of the references to color in this figure legend, the reader is referred to the web version of this article.)

silicon (powder, 99.9%, Aldrich), ruthenium (sponge, 99.95%, Alfa Aesar), and boron (crystalline pieces, 99.999%, J&M) were weighed in the $Ti_{3-x}Si_xRu_5B_2$ (x=0.25, 0.50, 0.75, 1.00, and 1.25) stoichiometric ratios (total mass 300 mg), pressed into pellets, and arc melted for 10 s each time. The samples were turned and melted several times to ensure good homogeneity. Weight losses during the melting process were less than 1%. The same procedure was used to synthesize a sample of nominal composition $V_2SiRu_5B_2$. The products were not sensitive to air or moisture.

2.2. Phase and chemical composition analyses

The samples were initially examined by powder X-ray diffraction for identification and phase purity on a Rigaku powder diffractometer employing Cu$K\alpha$ radiation (λ=1.5406 Å). The scattered intensity was recorded as a function of Bragg angle (2θ) using a scintillation detector with a step of 0.04° 2θ in step scan mode, ranging from 5° to 90°. Phase identification was made, and lattice parameters were refined by a full-profile Rietveld refinement [14] using LHPM RIETICA [15], on ground samples, from peaks between 20° and 60° in 2θ. The chemical composition was analyzed by an FEI Quanta 200 FEG Environmental SEM with voltage at 20 kV; spectra were collected for 100 s.

2.3. Structure determination

Single crystals selected from partially crushed polycrystalline samples were mounted on the tips of glass fibers. Room temperature intensity data were collected on a Bruker Apex II diffractometer with Mo radiation $K\alpha_1$ (λ=0.71073 Å). Data were collected over a full sphere of reciprocal space with 0.5° scans in ω with an exposure time of 10 s per frame. The 2θ range extended from 4° to 60°. The SMART software was used for data acquisition. Intensities were extracted and corrected for Lorentz and polarization effects with the SAINT program. Empirical absorption corrections were accomplished with SADABS, based on modeling a transmission surface by spherical harmonics employing equivalent reflections with $I > 2\sigma(I)$ [16,17]. Within the SHELXTL package, the crystal structures were solved using direct methods and refined by full-matrix least-squares on F^2 [18]. All crystal structure drawings were produced using the program VESTA [19].

2.4. Magnetization measurements

The magnetization measurements were performed in a 1 T applied field using a superconducting quantum interference device (SQUID) magnetometer by Quantum Design, Inc., over a temperature range of 2–300 K. The samples were placed in plastic capsules for measurement. The magnetization is linearly proportional to applied fields for fields up to 5 T and thus the magnetic susceptibility is defined as $\chi = M/\mu_0 H$ where M is the measured magnetization in emu and $\mu_0 H$ is the applied field in Oe.

2.5. Resistivity measurements

The resistivity measurements were measured on a bar-shaped sample using a Quantum Design Physical Property Measurement System (PPMS) equipped with a ^{3}He cryostat from 0.4 to 300 K in zero applied field in the standard 4-probe configuration.

Download English Version:

https://daneshyari.com/en/article/7758713

Download Persian Version:

https://daneshyari.com/article/7758713

Daneshyari.com